

# The effect of heat treatment on the microstructure and diffusion of silver in pyrolytic carbon coatings



F. Cancino-Trejo<sup>a</sup>, M. Sáenz Padilla<sup>a</sup>, E. López-Honorato<sup>a,\*</sup>, U. Carvajal-Nunez<sup>b</sup>,  
J. Boshoven<sup>b</sup>, J. Somers<sup>b</sup>

<sup>a</sup> Centro de Investigación y de Estudios Avanzados del IPN (CINVESTAV), Unidad Saltillo, Av. Industria Metalúrgica 1062, Ramos Arizpe, 25900, Mexico

<sup>b</sup> European Commission, Joint Research Centre, Institute for Transuranium Elements, PO Box 2340, D-76125, Karlsruhe, Germany

## ARTICLE INFO

### Article history:

Received 2 May 2016

Received in revised form

4 August 2016

Accepted 5 August 2016

Available online 6 August 2016

## ABSTRACT

It is well accepted that TRISO (tristructural isotropic) coated nuclear fuel particles are capable of retaining fission products up to 1600 °C, however above this temperature fission products can diffuse through the pyrolytic carbon (PyC) and silicon carbide coatings that act as the containment barriers in this fuel. Despite decades of research and development, little is known on the origin of this fuel temperature limit. In order to understand the origin of this fuel temperature PyC coatings produced by fluidized bed chemical vapor deposition were heat treated at 1000 °C, 1400 °C and 1700 °C for 200 h in an inert atmosphere. We have observed that above 1400 °C the anisotropy, domain size and level of graphitization increases to twice its original value. Furthermore, at 1700 °C some samples exhibited the formation of nano-pores, which could be the origin of the maximum fuel temperature limit or at least contribute to it. The increased diffusivity of elements due to microstructural changes was corroborated by silver diffusion experiments. Furthermore, we have observed that not all the samples suffer the same level of graphitization, thus suggesting that some PyC coatings can maintain their capability to retain fission products even after temperature excursions above 1600 °C.

© 2016 Elsevier Ltd. All rights reserved.

## 1. Introduction

The nuclear accident at Fukushima in March 2011 made evident the necessity of nuclear fuels with even higher tolerance to off-normal conditions. The TRISO (Tristructural Isotropic) coated fuel particles are among the options currently under study as accident tolerant fuels (ATF), and are an integral component contributing to the inherent safety of the High and Very High Temperature Reactors (HTR and VHTR). This type of fuel, first originated in the UK in the 1970s, is made of a uranium kernel coated with four layers of pyrolytic carbon (PyC) and one of silicon carbide (SiC) that operate as a miniature fission product (FP) containment vessel [1]. The kernel not only provides the energy in form of heat but also (partially) retains FP. The kernel is coated by a porous PyC coating layer, also described as the buffer, which attenuates fission recoil atoms and provides a void volume to accommodate gaseous fission products (e.g. krypton and xenon) and carbon monoxide. A dense

internal PyC coating layer (IPyC) is deposited on top of the buffer layer, sealing this porous structure and acting as a containment of gaseous and metallic FP (e.g. Sr-90 and Cs-137). This dense PyC also prevents the chemical attack of the kernel during the production of the SiC layer, and gives a higher mechanical stability to SiC by introducing a compressive stress during irradiation. The SiC layer is the main diffusion barrier of metallic FP and provides most of the mechanical properties of the fuel. Finally, the outer PyC coating layer (OPyC) is the last diffusion barrier and ensures the SiC is under compression during irradiation. The purpose of these coatings is to stop the release of all fission products even under abnormal operating conditions [2–6].

In order to ensure the safe containment of all important radionuclides, the maximum operating temperature of this fuel has been set at 1600 °C. This temperature was established after experimental results showed that some FPs start to be released above this temperature. Although this value is well established, little is known on the origin of the release of FP at this temperature, especially if it is considered that the decomposition of the constituents of the fuel is expected to occur at temperatures above 2000 °C [7,8]. Therefore, to understand and even increase even further the safety of this type

\* Corresponding author.

E-mail address: [eddie.lopez@cinvestav.edu.mx](mailto:eddie.lopez@cinvestav.edu.mx) (E. López-Honorato).

of fuel it is necessary to study in separate effect investigations the behavior of the ceramic coatings under off-normal conditions.

The PyC coatings used on TRISO particles are produced by fluidized-bed chemical vapor deposition (FBCVD, vertical machine) by the thermal decomposition of different hydrocarbons such as methane, propane, ethane, ethylene, acetylene, propylene, benzene, toluene, etc, using a deposition temperature between 900 and 1400 °C [9]. In the case of PyC, it is known that most of the physical properties change with their microstructure and this depends of the deposition conditions used in its preparation. Since it is possible to vary the deposition conditions such as temperature, volume/surface ratio, residence time and precursor concentration, different types of microstructures can be deposited on the fuel particle. Furthermore, when PyC receives a heat treatment above its deposition temperature, it undergoes a structural change evolving towards a more ordered structure similar to graphite, called graphitization [10]. As a result, the average size of the basal graphene planes and stacking thickness increase ( $L_a$  and  $L_c$ , respectively), whereas the interplanar distance ( $d_{002}$ ) and the curvature of graphene layers (tortuosity) decrease [11–15]. The effects of the heat treatment on PyC also can change its anisotropy (orientation of the graphene planes) [16].

The anisotropy (degree of preferential orientation of graphene planes) of PyC is an important property since it is strongly related to the probability of failure under neutron irradiation. As PyC is neutron irradiated it expands and contracts between and along the graphene planes, respectively. Therefore, if PyC is strongly oriented (anisotropic), it will tend to develop a higher shrinkage along the graphene planes and result in the formation of cracks that would result in the failure of the coating system and the release of fission products [17]. Consequently, the characterization of the anisotropy or texture is of critical importance for fuel licensing. Depending on the sampling area the texture of the material can be identified as nano (below 0.2  $\mu\text{m}$ ), micro (above 0.2  $\mu\text{m}$  and up to several tens of micrometers) or macro-texture (covering up to several millimeters), each one providing valuable information for the identification of possible failure under irradiation [18].

The microstructure of PyC and SiC coatings is one of the most important parameters that control the release of FP; therefore it is necessary to improve the understanding of the behavior of the different ceramic components at high temperature. Since the IPyC layer retains most of the FP and protect the SiC layer from chemical attack of some metallic FP and oxidizing gases [1,9], we have centered our work on studying the effect of temperature on the microstructure of this material, particularly at temperatures up to 1700 °C, and relating these results to the origin of the 1600 °C fuel temperature limit.

## 2. Experimental

### 2.1. Sample preparation

Seven different single layer PyC coatings were deposited by fluidized-bed chemical vapor deposition (FBCVD), using zirconia particles 500  $\mu\text{m}$  in diameter as substrate. Acetylene ( $\text{C}_2\text{H}_2$ ) (50% and 33%, v/v concentration) and a mixture of acetylene/propylene ( $\text{C}_2\text{H}_2/\text{C}_3\text{H}_6$ ) (33% and 25% v/v concentration) were used as precursor gases, together with Argon as fluidization gas. The general deposition conditions of each coating are listed in Table 1. Deposition conditions were selected to produce a wider range of densities. Samples were heat treated at 1000, 1400, and 1700 °C for 200 h under an argon atmosphere.

The samples were then embedded in copper-loaded resin and ground with successive grades of silicon carbide paper to the cross section, and then were polished down to 0.25  $\mu\text{m}$  diamond paste

grit. Finally, these samples were cleaned with water and ethanol in an ultrasonic bath prior to characterization.

For the silver diffusion experiments, PyC coatings were dip coated in a solution of colloidal silver (SPI SUPPLIES, dotite D-550), following another dip coating in a solution containing polycarbosilane (PCS, Nabond) in xylene (Jalmek). The samples were then heat treated up to 800 °C in an argon atmosphere to transform PCS into amorphous SiC. A detailed description of the preparation of this layer can be found elsewhere [3]. The deposition of an amorphous SiC layer allowed silver to be in direct contact with PyC during the diffusion experiment performed at 900 °C for 13 h in an argon atmosphere.

### 2.2. Sample characterization

#### 2.2.1. Crystal size

Crystal size or domain size was determined by X-ray diffraction (XRD) using a Philips X'Pert XRD instrument with a  $\text{Cu K}\alpha_1$  radiation source ( $\lambda = 1.5418 \text{ \AA}$ , 40 kV y 30 mA). The average domain sizes,  $L_c$  (between the graphene layers) and  $L_a$  (along the graphene layers) were estimated from the (002) and (100) reflections, respectively [15,19]. Samples were also characterized by Raman spectroscopy using a Jovin Yvon Horiba- Lab HR-800 Raman spectrometer, equipped with a 632.8 nm He–Ne laser source. Raman analysis was performed by single spot measurements using a 50x objective lens.

#### 2.2.2. Microstructure

The microstructure was characterized by Scanning Electron Microscopy (SEM; JEOL JSM-6300 system), and its composition by Energy Dispersive Spectroscopy (EDS, NORAN detector). Samples were also analyzed by Transmission Electron Microscopy (TEM; FEI-TITAN 80300). Samples were prepared by focused ion beam milling using a FEI-QUANTA 200-3D. Furthermore, PyC density was measured by the Archimedes method in ethanol. It should be stated that the density of these coatings in the nuclear industry is generally measured using a density column [20].

#### 2.2.3. Anisotropy

The anisotropy of PyC was characterized by a two modulator generalized ellipsometry microscope (2-MGEM, Hinds Instruments) attached with a mercury lamp and a 522 nm filter. This technique allows the measurement of the diattenuation (N) and optical anisotropy factor (OPTAF) that are related to the anisotropy of PyC. A more detailed description of the equipment and technique can be found in Refs. [16,18].

Anisotropy was also evaluated by obtaining the selected area electron diffraction patterns (SAED) using transmission electron microscopy (TEM; FEI-TITAN 80300). Further information on the anisotropy of PyC using this technique can be found in Refs. [17,21].

**Table 1**  
General Deposition Conditions for PyC coatings produced by CVD in this study.

Sample	Temperature (°C)	Acetylene-PyC (%v/v)		Acetylene/ propylene- PyC (%v/v)
		50	33	
C1	1300		X	
C2	1200		X	
C3	1200			X
C4	1175		X	
C5	1400	X		
C6	1175			X

### 3. Results and discussion

#### 3.1. Domain size

##### 3.1.1. X-ray diffraction

Fig. 1 shows the diffraction patterns for PyC-C2 and its samples heat treated up to 1700 °C. In this image it is possible to observe that the intensity of a few reflections increase (particularly the 002 at 1700 °C), whereas its full width at half maximum (FWHM) decreases and the signals become sharper. Table 2 gives a more detailed summary of all changes occurring in the samples when analyzed by X-Ray diffraction. In general, as the heating temperature increased, the intensity of the (002) reflection for all samples increased too. The full width at half maximum (FWHM) decreased progressively in all cases; C6 showed the largest variation of FWHM of 2.42° (2-theta) to 0.58° (2-theta) at the end of heat treatment at 1700 °C, while C1 only changed from 2.50 to 1.06°. Furthermore, the (002) reflection sharpened and moved slightly to higher angles with increasing treatment temperature (as can be seen in the zoom carried out in Fig. 1, which is presented on the top right corner), with sample C6 exhibiting the biggest change, as the peak of the (002) reflection moved from 25.29° up to 26.06° 2-theta by the effect of heat treatment. These results suggest that PyC increased its degree of graphitization as the heating temperature increased [13,22].

The diffraction patterns obtained were used to calculate the domain size between and along the graphene planes,  $L_c$  and  $L_a$ , respectively (Figs. 2 and 3) [19,23]. Fig. 2 shows that  $L_c$  increased with heat treatment temperature, although at different rates depending on the sample. For example, whereas sample C5 had an increase from 2.98 nm to 6.13 nm as the sample was heat treated up to 1700 °C, sample C6 changed 4 times more from 3.36 nm to 14.06 nm. Furthermore, Fig. 2 shows that  $L_c$  does not change when samples are heat treated at 1000 °C, and show an increase on their domain size only above 1400 °C, having their strongest domain size increment at 1700 °C. It should be noted that although all the samples started with a similar  $L_c$  size, samples responded differently to the heat treatment received, thus suggesting that some samples graphitize at a lower rate or are more resistant to graphitization. The values of  $L_c$  and the effect on temperature is similar to those reported by Kaae [24], showing as-deposited  $L_c$  sizes between 2.9 and 3.4 nm, and further increase on domain size up to 10 nm after heat treatments of 1900 °C for 1 h.

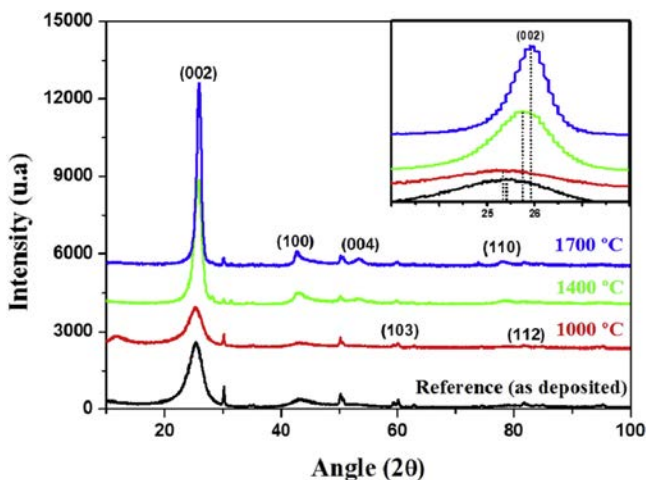


Fig. 1. X-Ray diffraction patterns for PyC-C2 coatings heat treated at various temperatures. A zoom of reflection (002) is displayed in the top right corner. (A colour version of this figure can be viewed online.)

Table 2

Changes analysis obtained by X-Ray diffraction for the PyC coatings.

Sample	Change before of heat treatment – After of heat treatment		
	Intensity (u. a)	FWHM (° (2θ))	Position (2θ)
C1	2265–6572	2.50–1.06	25.20–25.83
C2	2297–6559	2.65–1.01	25.54–25.86
C3	530–2166	2.42–0.87	25.29–26.03
C4	823–7424	3.53–0.92	25.17–25.96
C5	1452–2705	2.73–1.33	25.37–25.91
C6	2175–2670	2.42–0.58	25.29–26.06

The influence of heat treatment on the basal plane length,  $L_a$ , is shown in Fig. 3. As can be observed, the heat treatment caused an increase in  $L_a$  in all samples. However, once again samples with a similar starting  $L_a$  value responded differently to the heat treatment. Sample C5 increased  $L_a$  slightly from 2.28 nm to 3.43 nm at the end of heat treatment at 1700 °C. The same behavior was observed for sample C6, since it increased from 1.85 nm to 4.12 nm, twice its original value. Additionally, Fig. 3 shows that the samples with the highest initial crystal size were the least affected by the heat treatment, thus supporting the behavior already reported by other researchers [14]. It is possible that with higher initial crystal size, migration and annihilation of defects becomes more complicated [25]. Since the graphitization increases by the growth of well-ordered planes, as a 2-D propagation of ordering, ordered domains need a lateral expansion to create coherent domains, thus the size of the ordered domains increases by the elimination or migration of defects locked in small, disordered areas [19].

In the temperature range 25–1000 °C the domains only grow along the graphene planes ( $L_a$ ), whereas  $L_c$  remains almost unchanged (Figs. 2 and 3). This behavior was previously reported by Emmerich [26]. The coalescence of crystallites along the  $c$ - and  $a$ -axis is a thermally activated process that usually takes place at temperatures above 1400 °C. Domain size increases more readily when neighbouring domains already lie nearly parallel to each other [26]. This means that coatings with higher initial anisotropy would develop higher domain size growth than those with more isotropic structure. This is visible in sample C4 and C6 where domain size  $L_a$  (Fig. 3) grows at a higher rate than other coatings.

Before heat treatments, the  $sp^3$  and  $sp^2$  carbon bonds (hybridizations) coexist, however, the  $sp^3$  bond disappears with temperature, particularly at heat treatments above 1600 °C [27]. Therefore,

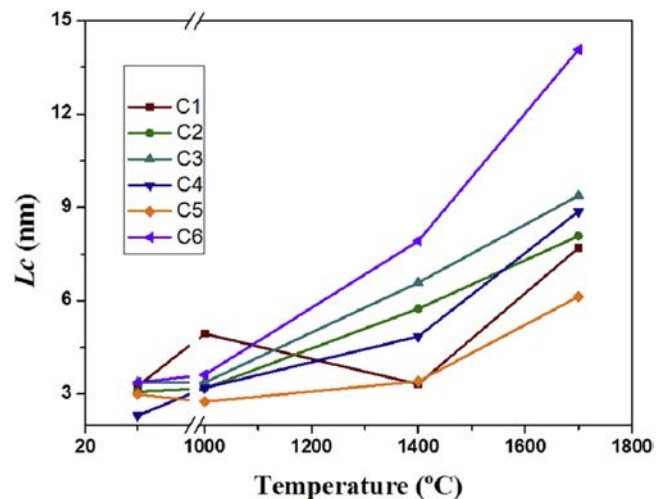
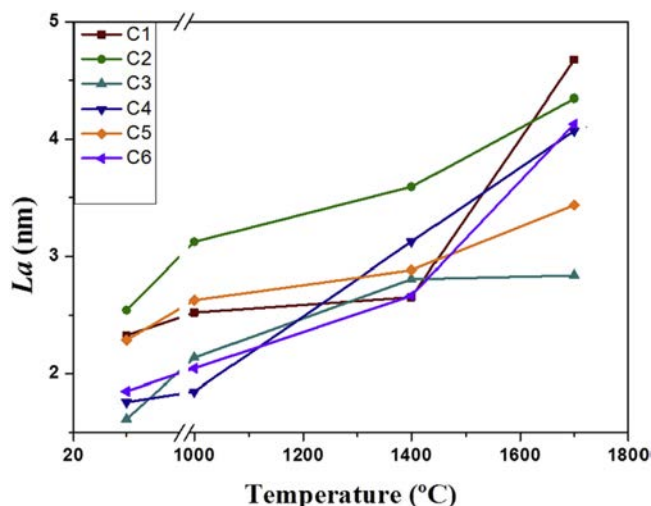


Fig. 2. Influence of heat treatment on the height of layer stacking ( $L_c$ ) of the PyC coatings. (A colour version of this figure can be viewed online.)

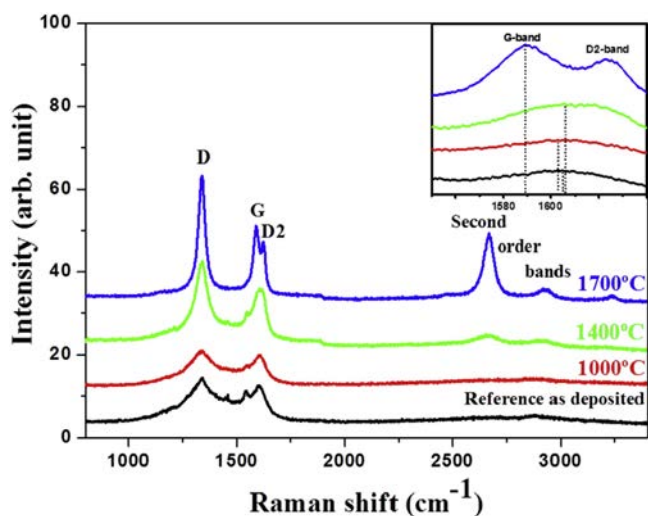


**Fig. 3.** Influence of heat treatment on the basal plane length ( $L_a$ ) of the PyC coatings. (A colour version of this figure can be viewed online.)

it is possible that the increase of domain size above 1400 °C could be due to the rearrangement of the graphene planes and the disappearance of the  $sp^3$  bonding. This is confirmed by X-Ray diffraction patterns, which indicated extensive narrowing of the (002) diffraction signal at this temperature (see Fig. 1), and the decrease of the width for D-band (Fig. 4) that is related to the growth of aromatic planes [28,29], thus resulting in a structure more similar to graphite with hybridization  $sp^2$  [27,30].

### 3.1.2. Raman spectroscopy

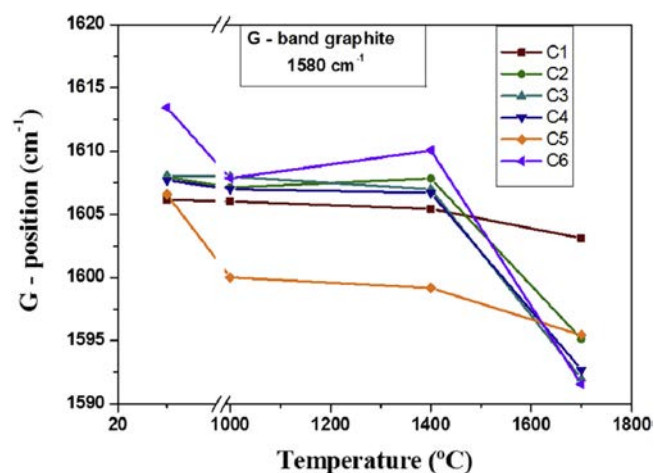
The Raman spectrum of crystalline graphite has only one peak at  $1580\text{ cm}^{-1}$  called the G-band. However, in the case of samples with some structural disorder, the breaking of the translational symmetry (e.g. edges impurities, size effects, etc.), permits an additional characteristic peak to be observed at around  $1350\text{ cm}^{-1}$ , called the D-band [27]. These bands are related to the degree of order along the graphene layers. Furthermore, second order bands appear above  $2700\text{ cm}^{-1}$ , which are related to the three dimensional arrangement along the crystallographic C-axis [31].



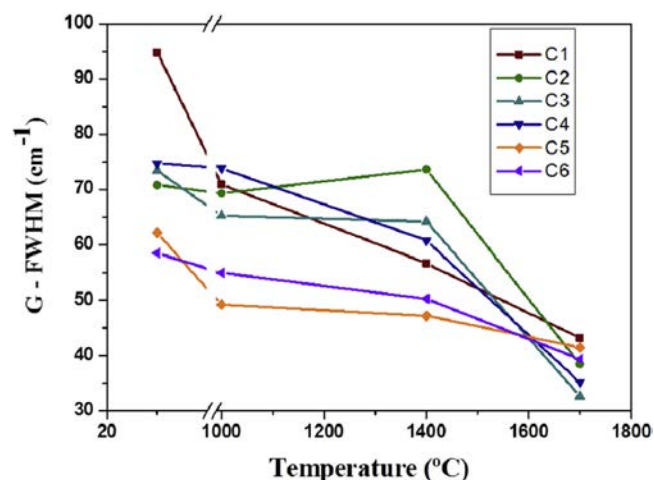
**Fig. 4.** Raman spectra for PyC coatings heat treated at various temperatures. A zoom of the G-band is displayed in the top right corner. (A colour version of this figure can be viewed online.)

Fig. 4 shows the Raman spectra obtained for different PyC coatings. In this image it is possible to observe that the intensity of the D, G and second order bands increase (particularly at 1700 °C), whereas the full width at half maximum (FWHM) decreases as the signals become sharper. The stronger intensity of the G-band indicate an increase of in-plane order in the graphic structure, and the decrease in the intensity at full width at half maximum (FWHM) in the D and G bands reveals the extent of the graphitization process [32]. Moreover, the D and G bands shift slightly towards lower energy. The D-band moved from  $1340\text{ cm}^{-1}$  to  $1337\text{ cm}^{-1}$ , whereas the G-band shifted from  $1613\text{ cm}^{-1}$  to  $1591\text{ cm}^{-1}$  (detail in Fig. 4), which is closer to the signal in graphite of  $1580\text{ cm}^{-1}$  (Fig. 5) [33,34]. Furthermore, this shift towards lower values of the G-band were only observed at temperatures above 1400 °C, with sample C6 showing once again the highest degrees of graphitization (Fig. 5).

The effect of temperature on the FWHM of the G-band (G-FWHM) is shown in Fig. 6. Overall, the G-FWHM decrease by increasing temperature, having only a minor change between 1000 and 1400 °C (remaining at around  $50\text{--}70\text{ cm}^{-1}$ ), and a significant change only after the heat treatment at 1400 °C with values reducing to  $40\text{ cm}^{-1}$ . Furthermore, although the as-produced material had different values of G-FWHM, after heat treatment at



**Fig. 5.** Effect of temperature on the energy of the G-band in Raman spectra of the PyC coatings. (A colour version of this figure can be viewed online.)



**Fig. 6.** Effect of temperature on the change in G band -FWHM in the Raman spectrum of PyC coatings. (A colour version of this figure can be viewed online.)

1700 °C all of them had values close to 40 cm<sup>-1</sup>. These results suggest an increase on the degree of graphitization of PyC, which is supported by the findings from XRD (see Fig. 1).

As the heat treatment increased up to 1700 °C, the D2 band appeared at 1624 cm<sup>-1</sup> next to the G band. The appearance of this band is related to an improvement in the stacking order along the C-axis. The G-band changes in shape, position and intensity depending on the stacking of the graphene planes [34]. If the heat treatment increased the degree of stacked graphene layers, the breathing mode of the sp<sup>2</sup> atoms would be more limited, since the stacking will produce a greater compaction and the stretching mode will be the dominant mode of vibration in the structure [29,34]. The decrease of FWHM of the G band is related to the stretching of the graphene planes, resulting from an increase in domain size [21]. The appearance of the second order bands above

2700 cm<sup>-1</sup> along with the decrease of the FWHM of the D (not shown) and G bands and the displacement of the G band towards values similar to graphite, at heat treatments of 1700 °C, suggests that PyC is transforming towards the formation of a more graphitic structure, although not at the same rate for all samples. This interpretation is fully consistent with the information found by XRD.

### 3.2. Anisotropy

#### 3.2.1. Ellipsometry

Table 3 shows the average diattenuation values (micro-texture measured by the degree of residual polarization of light after interaction with de surface) of each PyC coating as well as its corresponding Optical Anisotropy Factor (OPTAF). The diattenuation and OPTAF values of as-deposited PyC varied from 0.010 to 0.014 and 1.020 to 1.030, respectively. The diattenuation and OPTAF values for all as-deposited samples were below the maximum permitted values of 0.02 and 1.04, respectively. This threshold indicates a sudden increase of failure risk probability from zero to 50% under neutron irradiation [18].

Additionally, in Table 3, it can be seen that the diattenuation and OPTAF of PyC coatings increased significantly after heat treatment at 1700 °C. Samples C2, C4 and C6 reached values higher than the recognized maximum limit of N ~0.02 (OPTAF ~ 1.04), i.e. N 0.022–0.037 and OPTAF of 1.056–1.078, respectively. The sample which showed the greatest increase in diattenuation and OPTAF after heat treatment was C6 since its diattenuation went from 0.014 to 0.037 and its OPTAF correspondingly from 1.030 to 1.078.

**Table 3**

Diattenuation and OPTAF values obtained by ellipsometry for PyC coatings heat treated to various temperatures.

Sample - heat treatment (°C)	Diattenuation	OPTAF
C1 – 1700 °C	0.011 ± 0.005	1.022
C2 – as deposited	0.011 ± 0.005	1.022
C2 – 1700 °C	0.025 ± 0.013	1.052
C3 – as deposited	0.011 ± 0.005	1.023
C4 – as deposited	0.013 ± 0.006	1.026
C4 – 1700 °C	0.022 ± 0.011	1.046
C5 – as deposited	0.010 ± 0.003	1.020
C5 – 1700 °C	0.011 ± 0.005	1.021
C6 – as deposited	0.014 ± 0.006	1.030
C6 – 1700 °C	0.037 ± 0.018	1.078

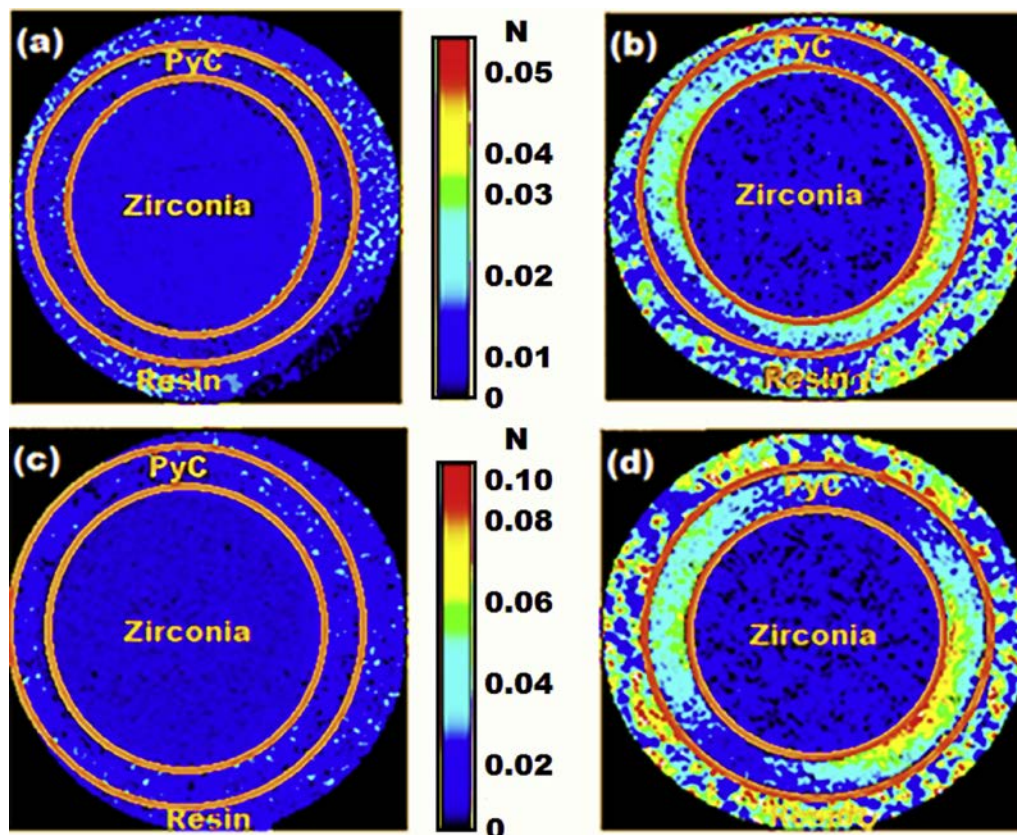


**Fig. 7.** Diattenuation maps of single PyC coatings (a, b) sample C2 (as-deposited, and at the end of heat treatment to 1700 °C, respectively) and (c, d) sample C6 (as-deposited and at the end of heat treatment to 1700 °C). In the scale that is in the center the red is the scale maximum and black is the scale minimum. (A colour version of this figure can be viewed online.)

Conversely, sample C5 suffered the lowest change, as  $N$  went from 0.010 to 0.011 and OPTAF from 1.020 to 1.021. This trend is consistent with XRD and Raman spectroscopy, which showed that sample C5 and C6 had the lowest and greatest increase in domain size  $L_c$ , respectively, despite both having almost the same initial value when produced.

These important changes in anisotropy after heat treatment can be seen in the diattenuation maps and histograms in Figs. 7 and 8. It is important to notice that although the average value of diattenuation after heat treatment at 1700 °C in sample C2 was 0.025, the diattenuation is not uniform since the coating has areas with diattenuation as high as 0.05 (Fig. 7b). This behavior can also be observed in Fig. 8a and b, where there is a distribution width beyond the average values (0.011 and 0.025 for as-deposited and after heat treatment at 1700 °C, respectively). These results show the lack of a uniform distribution of anisotropy in this type of coatings. The distribution of the diattenuation in Fig. 8a, b, c and d indicates that although the average value of anisotropy in PyC is less than  $N \sim 0.02$  or OPTAF  $\sim 1.04$  (Fig. 8a and c), there might be areas that would exceed this limit, and therefore would be susceptible to cracking under neutron irradiation and off-normal operating conditions. This is important since an initial average value of low anisotropy is not a guarantee for survival under off-normal conditions. Furthermore, these 2-MGEM results confirm that the samples with the highest initial crystal size were the least affected by the heat treatment (for example sample C5).

As was observed by Raman Spectroscopy and XRD, not all the samples had the same increase in anisotropy. For example, sample C6 had  $\sim 150\%$  increase from 0.0148 to 0.0374, whereas sample C5 only had  $\sim 0.1\%$  increase from 0.010 to 0.011. This suggests that some samples can resist temperatures above 1700 °C with lower changes in their microstructure. This could be related to the orientation of

the graphene planes in the as-produced coatings. As it has been previously shown, different deposition conditions will result in different microstructures (globular or polyhedral structures) with considerably different graphene orientation [18]. In accordance with Raman Spectroscopy and XRD, sample C5 had a large initial domain size, and a lower diattenuation as confirmed by 2-MGEM. After each heat treatment, sample C5 showed the lowest effect from temperature ( $L_a$ ,  $L_c$ , OPTAF, density, etc.), therefore sample C5 is considered the most resistant towards graphitization.

### 3.3. Density

The effect of temperature on the density of the PyC coatings is shown in Fig. 9. Overall, it can be observed that density decreased slightly with heat treatment temperature. It should be noted that samples C2, C3, C4 and C6 started with similar density above 2.2 g/cm<sup>3</sup>, whereas samples C1 and C5 started with densities of 2.00 and 1.72 g/cm<sup>3</sup>, respectively. Sample C1 showed the largest variation of density from 2.00 to 1.89 g/cm<sup>3</sup> at the end of heat treatment at 1700 °C, while sample C5 only changed from 1.72 to 1.70 g/cm<sup>3</sup>. It is important to mention that the decrease of density is observed for dense (samples C1–C4 and C6) and more porous structures (sample C5).

Practically, all samples remained above of the 1.8 g/cm<sup>3</sup> even after heat treatment at 1700 °C (C1, C2, C3, C4 and C6). Only C5 had a lower value of density before the heat treatment, changing only approximately 1.5%. Once again, it should be noted that although some samples started with a similar density, samples responded differently to the heat treatment, thus suggesting that some samples graphitize at a lower rate or are more resistant to graphitization.

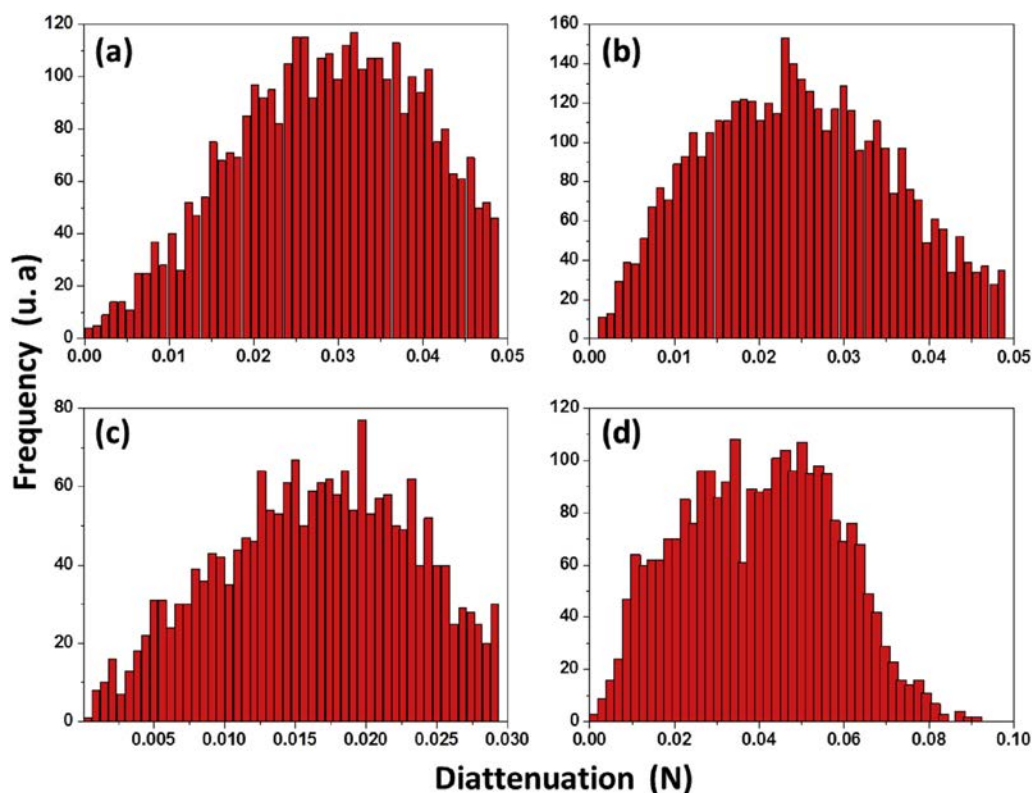
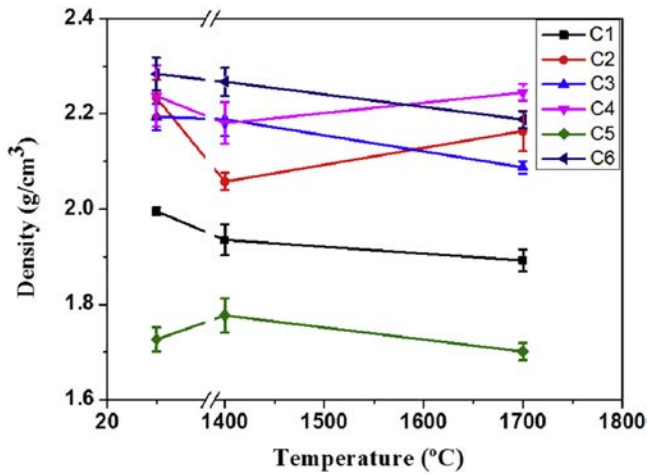


Fig. 8. — Histograms of the diattenuation ( $N$ ) of single PyC coatings (a, b) sample C2 (as-deposited, and at end of heat treatment to 1700 °C, respectively) and (c, d) sample C6 (as-deposited and at end of heat treatment to 1700 °C). (A colour version of this figure can be viewed online.)



**Fig. 9.** Influence of heat treatment on the density of the PyC coatings. (A colour version of this figure can be viewed online.)

### 3.4. Microstructure

#### 3.4.1. Optical and scanning electron microscopy

Fig. 10 is an image obtained by optical microscopy for the sample C2, showing a homogeneous PyC coating with a small amount of porosity larger than  $0.5 \mu\text{m}$  (Fig. 10a) and density  $\approx 2.2 \text{ g/cm}^3$  (see Fig. 9). As the sample was heat treated at  $1700 \text{ }^\circ\text{C}$ , its density decreased slightly until  $\approx 2.1 \text{ g/cm}^3$  (see Fig. 9) and the large porosity disappeared, giving the appearance of a more granular

coating (Fig. 10b).

Fig. 11 shows micrographs of the fracture surface of sample C6 before and after heat treatment at  $1700 \text{ }^\circ\text{C}$ . The as-deposited samples were composed of a dense globular type structure, with globular features of about  $1 \mu\text{m}$  (Fig. 11a). However, after the  $1700 \text{ }^\circ\text{C}$ , the microstructure turned into a mixture of globular and laminar structures (Fig. 11b). The laminar character is more related to anisotropic PyC coatings [18,31], also supporting the finding from Raman spectroscopy and XRD that suggests that heat treatments at  $1700 \text{ }^\circ\text{C}$  produced more graphitic structures.

#### 3.4.2. Transmission electron microscopy (TEM)

Fig. 12 shows the high resolution transmission electron micrographs and diffraction patterns of PyC before and after heat treatments at  $1700 \text{ }^\circ\text{C}$ . Before heat treatment, samples C2 and C6 (Fig. 12a and c, respectively) had graphene planes with a degree of disorder and randomness. Additionally, the graphene layers exhibit some tortuosity and small extent of stacking among graphene planes. At the end of heat treatment at  $1700 \text{ }^\circ\text{C}$ , the domain size and the number of stacked graphene layers increased, in addition to a decrease on the tortuosity of the graphene. Furthermore, it is possible to observe a better alignment of the graphene layers and an increase in the overall preferred orientation after heat treatment (see Fig. 12b and d). As shown in the TEM micrographs, sample C6 has a strong change in graphene alignment as confirmed by its diffraction patterns which show the (002) diffractions signals when heat treated at  $1700 \text{ }^\circ\text{C}$  (Fig. 12c and d). Based on the orientation angle (OA) samples showed changes in its anisotropy; sample C2 changed from  $\text{AO} = 47^\circ$  to  $\text{AO} = 35^\circ$ , whereas C6 changed from  $\text{AO} = 37^\circ$  to  $29^\circ$  (see Fig. 12a, b, c and d), both samples achieving an

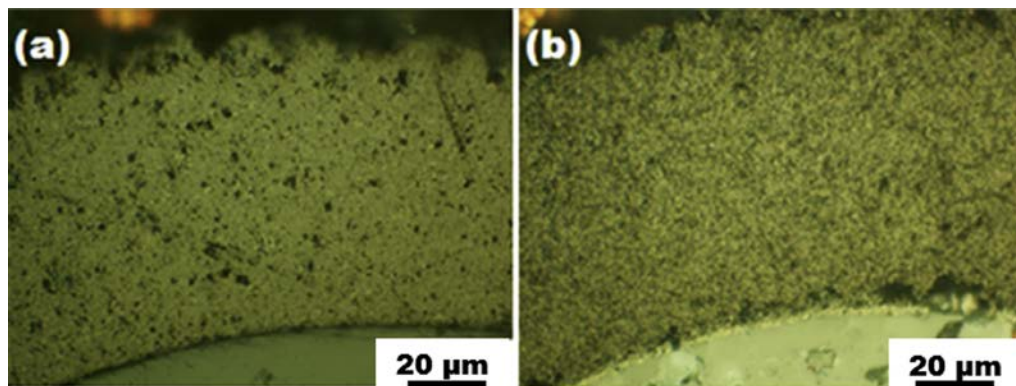


**Fig. 10.** Images of PyC coatings obtained by optical microscopy (a) sample C2 as-deposited and (b) sample C2 after heat treatment at  $1700 \text{ }^\circ\text{C}$ . In the image smaller pores are now visible at the end of heat treated at  $1700 \text{ }^\circ\text{C}$ . (A colour version of this figure can be viewed online.)

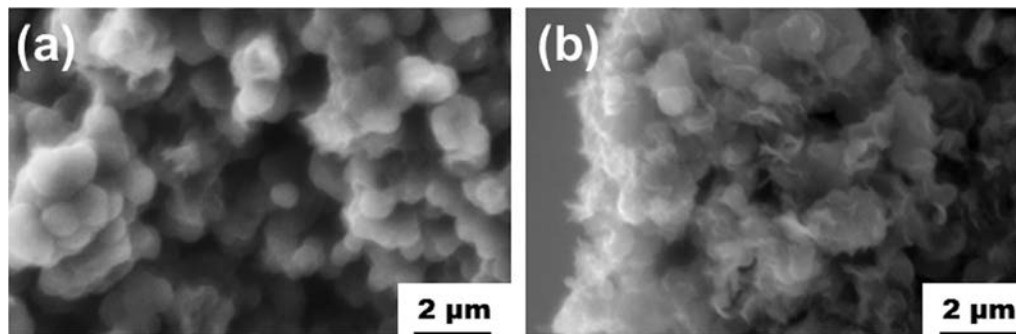


**Fig. 11.** Image of PyC coating obtained by SEM (a) C6 without heat treatment as-deposited, (b) C6 after heat treatment at  $1700 \text{ }^\circ\text{C}$ .

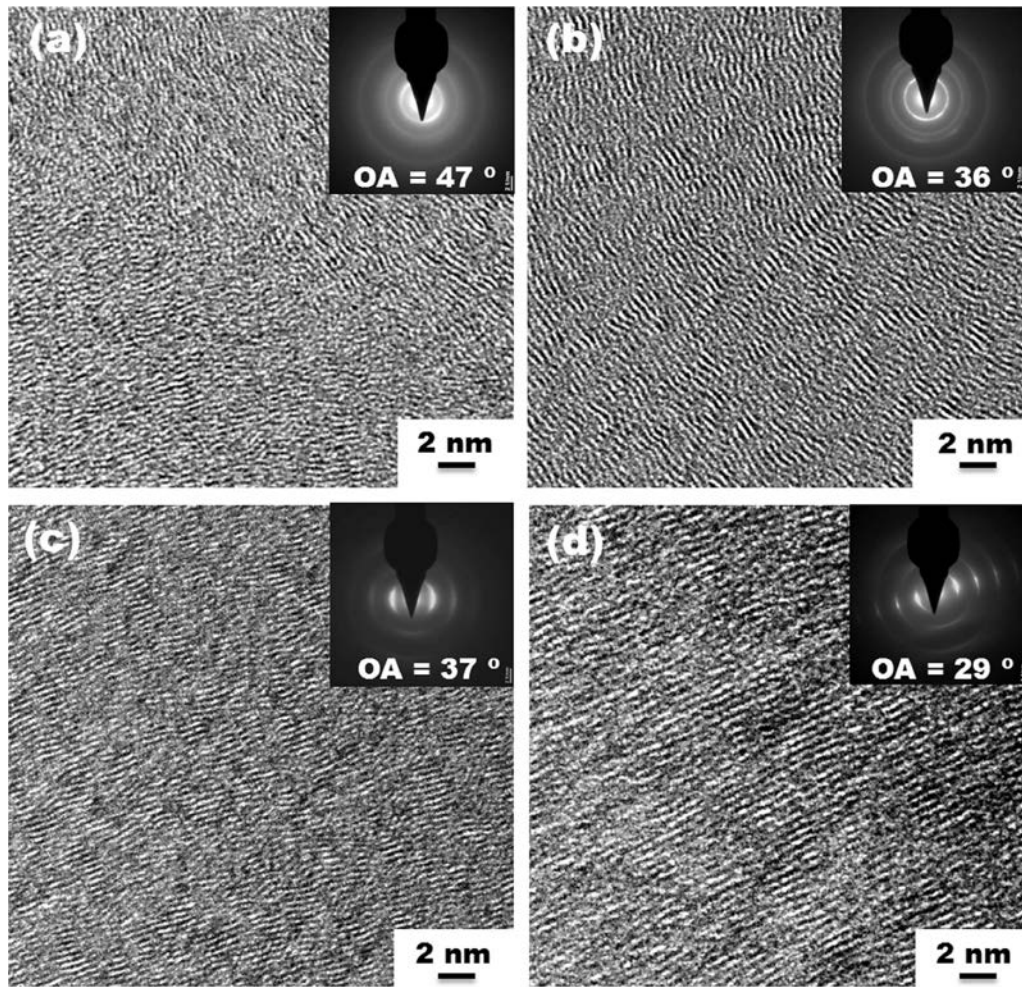


**Fig. 12.** TEM high-resolution images exhibiting differences in the characteristics of the graphene layers as  $L_a$ ,  $L_c$ , tortuosity and anisotropy by effect of temperature. Left (samples C2 and C6, without heat treatment as-deposited, (a) and (c), respectively), right (samples C2 and C6, heat treatment at 1700 °C, (b) and (d), respectively).

anisotropy degree which correlates to a high-texture (according to recently suggested terminology, on which the high textures (HT) were designated by OA 0–50°, medium (MT) 50–80° and low (LT) 80°+) [35].

In addition to the changes observed in the graphene planes, a very important observation is the development of what appears to be cracks or porosity in the microstructure of PyC after heat treatment at 1700 °C (Fig. 13). This is very relevant because the formation of cracks or porosity could lead to a higher degree of diffusion of fission products, thus reducing the efficiency of this material to contain these elements during off-normal conditions. It is important to mention that these cracks or pores were not seen in samples heat treated at 1400 °C. This porosity could be the result of the increase of anisotropy and graphitization, as well as the increase of domain size and the responsible for the slight decrease in density observed. Fig. 14a, b and c shows a possible route to the formation of these nano-cracks or nano-porous. When samples are randomly oriented or contain tortuosity, these graphene planes will occupy a certain volume (Fig. 14a). As the graphene planes grow and align above 1400 °C, the same number of graphene planes will occupy a lower volume, thus leaving gaps between domains that will combine to form nano-pores (Fig. 14b). The increase of graphitization and the formation of these pores around 1700 °C could be the origin of the increase of diffusion of fission products, and are potentially the cause of the 1600 °C temperature limit in

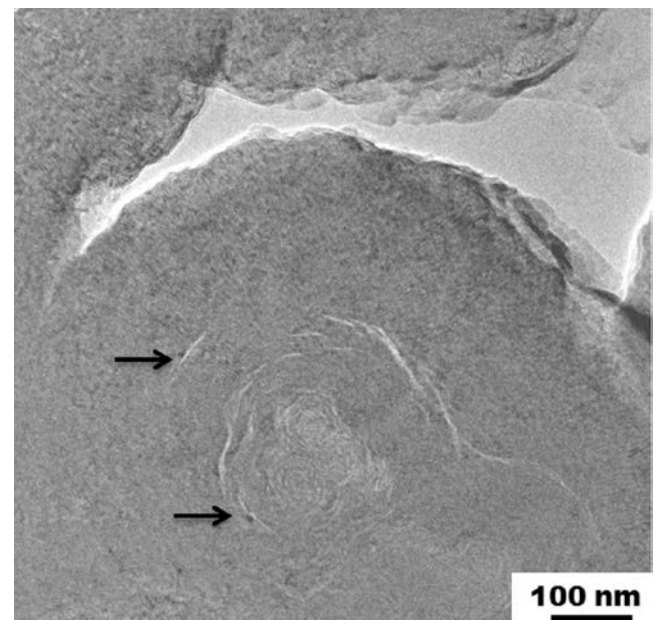


**Fig. 13.** TEM low-resolution image showing the presence of porosity (as indicated by the black arrows) result of microstructural changes or graphitization of the PyC coatings at end of heat treatment of 1700 °C.

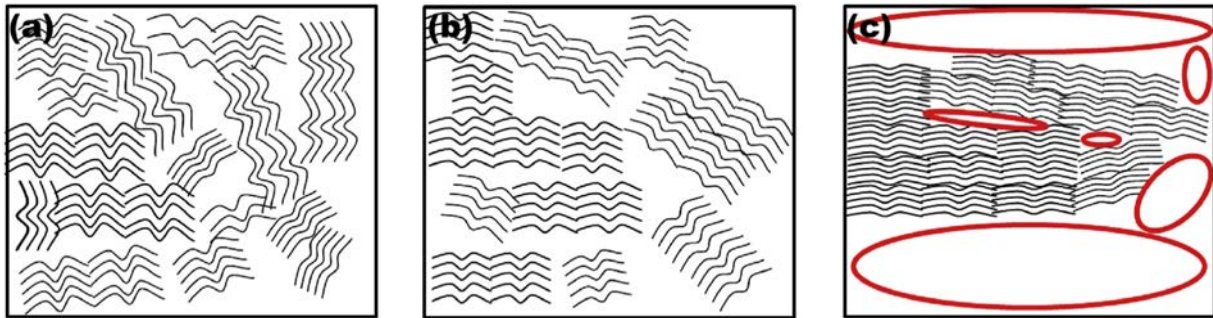


**Fig. 14.** Formation of nano-pores by effect of heat treatment. (a) as-deposited, (b) heat treatment at 1400 °C, and (c) at end of heat treatment of 1700 °C. The red zones in (c) indicate the occupied volume reduction by effect of the graphitization of the PyC coatings; this in turn creates gaps between domains that will combine into the formation of nano-pores. (A colour version of this figure can be viewed online.)

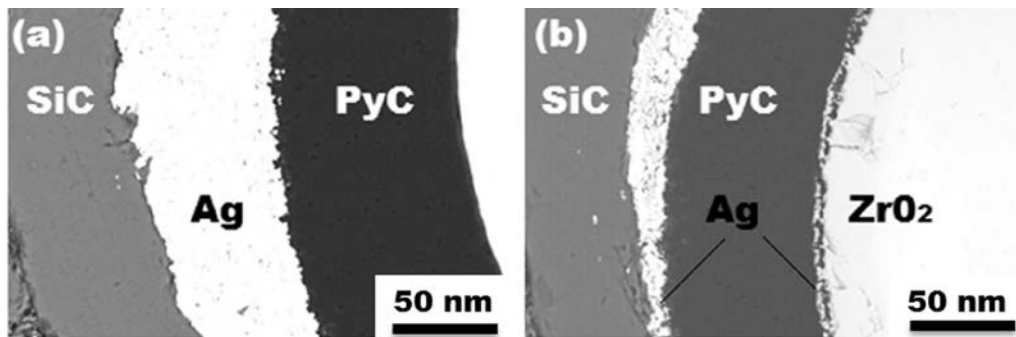


**Fig. 15.** SEM images showing samples heat treated for diffusion tests at 900 °C (a) as-deposited C6; (b) C6 coating heat treated at 1700 °C for 200 h after diffusion tests.

the use of TRISO coated particles. Since together with the kernel, the buffer and the IPyC retain the largest amount of fission products in the TRISO particles [36], the formation of pores will allow the diffusion of elements that could chemically attack SiC [37], thus making it permeable and resulting in the continuous increase of diffusion and release of fission products at higher temperatures.

### 3.5. Silver diffusion in PyC coatings

In order to prove that the changes in microstructure in PyC could result in higher diffusion rates of even metallic fission products, we tested the diffusion of silver in these coatings (Fig. 15). Fig. 15a show the diffusion couples prepared where silver was trapped between a layer of PyC and SiC. Our results show that Ag did not clearly diffuse through as-deposited PyC during a diffusion test at 900 °C for 13 h (Fig. 15a). However, when the same experiment was repeated with a coating heat treated at 1700 °C, Ag completely diffused through PyC and was found at the zirconia/PyC interface (Fig. 15b), as confirmed by EDS (not shown). Our results suggest that heat treatments at 1700 °C not only produce important changes in microstructure and level of graphitization, but also that these changes are reflected in the formation of a more permeable PyC. Since PyC retains a large proportion of fission products, the change in this property could mean that many other fission products could more easily diffuse through this layer and probably even interact with SiC, reducing also its containment capacity.

## 4. Conclusion

In this work we study the origin of the increased release of fission products in TRISO particles above 1600 °C. Since the three PyC coatings that compose this fuel retain most of the fission products we centered our study on the effect of annealing

temperature on different types of PyC coatings produced by fluidized bed chemical vapor deposition. We observed that regardless of the deposition conditions all samples increased their graphitization level. However, some samples are affected less, thus retaining to some extent their original structure and level of disorder. Heat treatment of PyC coatings causes an increase in the anisotropy, domain size and degree of stacking of graphene layers and a decrease in the tortuosity of the graphene layers. The graphitization level increased considerably above 1400 °C. Therefore our results suggest that the origin of the 1600 °C temperature limit of TRISO particles is strongly related to microstructural changes happening to PyC. This is supported by the observation of the formation of nano-pores in samples heat treated at 1700 °C. Since the function of PyC is to retain a large proportion of fission products, and also protect SiC from interacting with them (particularly metallic elements such as Pd and Fe), the sudden increase of diffusion rates might hinder the capability of SiC to also contain fission products, thus lowering the overall retention capability of this coating system.

## Acknowledges

This material is based upon work supported by a grant from the University of California Institute for Mexico and the United States (UC MEXUS) and the Consejo Nacional de Ciencia y Tecnología de México (CONACYT). The authors would like to acknowledge the financial support provided by CONACYT and UC MEXUS-CONACYT for a PhD and BSc scholarship awarded to F. Cancino-Trejo and M. Sáenz Padilla, respectively.

## References

- [1] H. Nickel, H. Nabilek, G. Pott, A. Mehner, Long time experience with the

- development of HTR fuel elements in Germany, *Nucl. Eng. Des.* 217 (1) (2002) 141–151.
- [2] K. Minato, T. Ogawa, S. Kashimura, K. Fukuda, M. Shimizu, Y. Tayama, et al., Fission product palladium-silicon carbide interaction in htgr fuel particles, *J. Nucl. Mater.* 172 (2) (1990) 184–196.
- [3] E. López-Honorato, D. Yang, J. Tan, P.J. Meadows, P. Xiao, Silver diffusion in coated fuel particles, *J. Am. Ceram. Soc.* 93 (10) (2010) 3076–3079.
- [4] H. Zhang, E. López-Honorato, P. Xiao, Effect of thermal treatment on microstructure and fracture strength of SiC coatings, *J. Am. Ceram. Soc.* 96 (5) (2013) 1610–1616.
- [5] W. Schenk, A. Naoumidis, H. Nickel, The behaviour of spherical HTR fuel elements under accident conditions, *J. Nucl. Mater.* 124 (0) (1984) 25–32.
- [6] M.J. Kania, H. Nabielek, K. Verfondern, H.-J. Allelein, Testing of HTR UO<sub>2</sub> TRISO fuels in AVR and in material test reactors, *J. Nucl. Mater.* 441 (1–3) (2013) 545–562.
- [7] Y. Kurata, K. Ikawa, K. Iwamoto, Fission product release from Triso-coated UO<sub>2</sub> particles at 1940 to 2320°C, *J. Nucl. Mater.* 98 (1) (1981) 107–115.
- [8] K. Minato, T. Ogawa, K. Fukuda, H. Sekino, H. Miyanishi, S. Kado, et al., Release behavior of metallic fission products from HTGR fuel particles at 1600 to 1900°C, *J. Nucl. Mater.* 202 (1) (1993) 47–53.
- [9] A. Oberlin, Pyrocarbons, *Carbon* 40 (1) (2002) 7–24.
- [10] H. Saadaoui, J.C. Roux, S. Flandrois, B. Nysten, Graphitization of pyrocarbons: an STM study, *Carbon* 31 (3) (1993) 481–486.
- [11] S.B. Lyon, 3.24-Degradation of carbon and graphite, in: B. Cottis, M. Graham, R. Lindsay, S. Lyon, T. Richardson, D. Scantlebury, et al. (Eds.), *Shreir's Corrosion*, Elsevier, Oxford, 2010, pp. 2271–2281.
- [12] H. Takahashi, H. Kuroda, H. Akamatu, Correlation between stacking order and crystallite dimensions in carbons, *Carbon* 2 (4) (1965) 432–433.
- [13] M. Endo, Y.A. Kim, T. Hayashi, T. Yanagisawa, H. Muramatsu, M. Ezaka, et al., Microstructural changes induced in “stacked cup” carbon nanofibers by heat treatment, *Carbon* 41 (10) (2003) 1941–1947.
- [14] M. Guellali, R. Oberacker, M.J. Hoffmann, Influence of heat treatment on microstructure and properties of highly textured pyrocarbons deposited during CVD at about 1100°C and above 2000°C, *Compos. Sci. Technol.* 68 (5) (2008) 1122–1130.
- [15] A. Ramos, I. Cameán, A.B. García, Graphitization thermal treatment of carbon nanofibers, *Carbon* 59 (0) (2013) 2–32.
- [16] J.D. Hunn, G.E. Jellison Jr., R.A. Lowden, Increase in pyrolytic carbon optical anisotropy and density during processing of coated particle fuel due to heat treatment, *J. Nucl. Mater.* 374 (3) (2008) 445–452.
- [17] P.J. Meadows, E. López-Honorato, P. Xiao, Fluidized bed chemical vapor deposition of pyrolytic carbon – II. Effect of deposition conditions on anisotropy, *Carbon* 47 (1) (2009) 251–262.
- [18] E. López-Honorato, J. Boshoven, P.J. Meadows, D. Manara, P. Guillermier, S. Jühe, et al., Characterisation of the anisotropy of pyrolytic carbon coatings and the graphite matrix in fuel compacts by two modulator generalised ellipsometry and selected area electron diffraction, *Carbon* 50 (2) (2012) 680–688.
- [19] I. Rannou, V. Bayot, M. Lelaurain, Structural characterization of graphitization process in pyrocarbons, *Carbon* 32 (5) (1994) 833–843.
- [20] G.B. Engle, W.H. Norris, L. Bailey, Apparatus and procedure to determine density and structural distributions in carbons and graphites, *Carbon* 8 (3) (1970) 393–395.
- [21] X. Bourrat, Pyrocarbon performances and characterization, *Proc. Carbon* 11 (ID792) (2009).
- [22] M. Weisenberger, I. Martin-Gullon, J. Vera-Agullo, H. Varela-Rizo, C. Merino, R. Andrews, et al., The effect of graphitization temperature on the structure of helical-ribbon carbon nanofibers, *Carbon* 47 (9) (2009) 2211–2218.
- [23] G.A. Zickler, B. Smarsly, N. Gierlinger, H. Peterlik, O. Paris, A reconsideration of the relationship between the crystallite size *L*<sub>a</sub> of carbons determined by X-ray diffraction and Raman spectroscopy, *Carbon* 44 (15) (2006) 3239–3246.
- [24] J. Kaee, The effect of annealing on the microstructures and the mechanical properties of poorly crystalline isotropic pyrolytic carbons, *Carbon* 10 (6) (1972) 691IN3695–694IN5699.
- [25] J. Goma, A. Oberlin, Microtexture and structure of high temperature massive pyrocarbons prepared on graphite substrates, *Carbon* 23 (1) (1985) 85–90.
- [26] F. Emmerich, Evolution with heat treatment of crystallinity in carbons, *Carbon* 33 (12) (1995) 1709–1715.
- [27] L.G. Cañado, K. Takai, T. Enoki, M. Endo, Y.A. Kim, H. Mizusaki, et al., General equation for the determination of the crystallite size *L*<sub>a</sub> of nanographite by Raman spectroscopy, *Appl. Phys. Lett.* 88 (16) (2006).
- [28] M. Nakamizo, R. Kammereck, P.L. Walker Jr., Laser raman studies on carbons, *Carbon* 12 (3) (1974) 259–267.
- [29] A. Sadezky, H. Muckenhuber, H. Grothe, R. Niessner, U. Pöschl, Raman microspectroscopy of soot and related carbonaceous materials: spectral analysis and structural information, *Carbon* 43 (8) (2005) 1731–1742.
- [30] P. Tan, Y. Deng, Q. Zhao, Temperature-dependent Raman spectra and anomalous Raman phenomenon of highly oriented pyrolytic graphite, *Phys. Rev. B* 58 (9) (1998) 5435.
- [31] E. López-Honorato, P.J. Meadows, P. Xiao, Fluidized bed chemical vapor deposition of pyrolytic carbon – I. Effect of deposition conditions on microstructure, *Carbon* 47 (2) (2009) 396–410.
- [32] D.-S. Zhang, K.-Z. Li, H.-J. Li, L.-J. Guo, J.-H. Lu, The influence of deposition temperature on the microstructure of isotropic pyrocarbon obtained by hot-wall chemical vapor deposition, *J. Mater. Sci.* 46 (10) (2011) 3632–3638.
- [33] C.A. Taylor, M.F. Wayne, W.K.S. Chiu, Heat treatment of thin carbon films and the effect on residual stress, modulus, thermal expansion and microstructure, *Carbon* 41 (10) (2003) 1867–1875.
- [34] A.C. Ferrari, Raman spectroscopy of graphene and graphite: disorder, electron-phonon coupling, doping and nonadiabatic effects, *Solid State Commun.* 143 (1–2) (2007) 47–57.
- [35] B. Reznik, K.J. Hüttinger, On the terminology for pyrolytic carbon, *Carbon* 40 (4) (2002) 621–624.
- [36] H. Nabielek, W. Kühnlein, W. Schenk, W. Heit, A. Christ, H. Ragoss, Development of advanced HTR fuel elements, *Nucl. Eng. Des.* 121 (2) (1990) 199–210.
- [37] R.L. Pearson, R. Lauf, T. Lindemer, Interaction of Palladium, the Rare Earths, and Silver with Silicon Carbide in HTGR Fuel Particles, Oak Ridge National Lab, TN (USA), 1982.